Preliminary data on the energy distribution of X- and gamma-rays from natural lightning

Luis Contreras-Vidal[1], James T. Sanchez[1,3], Caitano L. da Silva[1], Richard G. Sonnenfeld[1], Graydon Aulich[1], Harald E. Edens[2], Kenneth B. Eack[2], David M. Smith[3]

[1]Department of Physics & Langmuir Lab, New Mexico Tech, Socorro, NM, USA
[2]Space and Remote Sensing, Los Alamos National Laboratory, Los Alamos, NM, USA
[3]Physics Department and Santa Cruz Institute for Particle Physics, University of California, Santa Cruz, CA, USA

Key Points:

- 5-ns resolution allowed for the measurement of individual X-ray photon energies from natural lightning and to confirm its power-law spectrum.
- Stepped leader X-rays come in a train of bursts lasting milliseconds, while dart leader X-rays come effectively in a single burst.
- Stepped leaders have a harder energy spectrum than dart leaders, with a larger population of >1 MeV photons.

Corresponding author: Luis Contreras-Vidal, `luis.contrerasvidal@student.nmt.edu`

Abstract

During the 2022 New Mexico monsoon season, we deployed two X-ray scintillation detectors, coupled with a 180 MHz data acquisition system to detect X-rays from natural lightning at the Langmuir Lab mountain-top facility, located at 3.3 km above mean sea level. Data acquisition was triggered by an electric field antenna calibrated to pick up lightning within a few km of the X-ray detectors. We report the energies of over 240 individual photons, ranging between 13 keV and 3.8 MeV, as registered by the $LaBr_3$(Ce) scintillation detector. These detections were associated with four lightning flashes. Particularly, four stepped leaders and seven dart leaders produced energetic radiation. The reported photon energies allowed us to confirm that the X-ray energy distribution of natural stepped and dart leaders follows a power-law distribution with exponent ranging between 1.09 and 1.96, with stepped leaders having a harder spectrum. Characterization of the associated leaders and return strokes was done with four different electric field sensing antennas, which can measure a wide-range of time scales, from the static storm field to the fast change associated with dart leaders.

1 Introduction

X-ray emissions from lightning were first discovered at Langmuir Lab by Moore et al. (2001) over twenty years ago. Moore et al. (2001) reported the discovery of X-ray photon energies up to 1.2 MeV associated with stepped lightning leaders. They also reported peak currents and electric field changes for three flashes that produced X-rays. Although the experimental setup employed by Moore et al. (2001) featured a high sampling rate of 1 MHz, they were unable to resolve energies of individual photons due to pile-up at the NaI(Th) scintillation detector. Photon pile-up refers to the situation where multiple photons arrive at the detector within a short time window (Pantuso et al., 2022). The width of this time window corresponds to the width of the voltage pulse registered in the data acquisition system, which in its turn is dictated by the decay time of the crystal and by the overall electronics of the detector. For a typical NaI(Tl) detector coupled with a photomultiplier tube (PMT), this time scale is of the order of 1 μs or longer. This inability to resolve pile-up due to long pulse duration persisted in the subsequent studies reviewed in this Introduction. NaI(Tl) scintillation detectors were deployed at Langmuir Lab every Summer, for several years, following the Moore et al. (2001) study. The additional data collected showed that dart leaders also produce X-rays (although not all in the same flash necessarily do), and that single-photons can have (up to) gamma energies (i.e., >1 MeV as evidenced by two co-located detectors displaying a single MeV photon detected by just one of them) (Eack et al., 2006).

Substantial knowledge on the nature of X-ray emissions from lightning leaders was gained through nearly two decades of investigations at the International Center for Lightning Research and Testing (ICLRT) in Camp Blanding, FL. Dwyer et al. (2003, 2004) reported that rocket-triggered lightning also emits bursts of X-rays and that the detected energetic radiation of triggered lightning X-rays extended up to about 250 keV in discrete bursts lasting less than 1 μs. Howard et al. (2008) confirmed the emission of X-rays from negative natural and rocket-triggered lightning strokes. Moreover, using time of arrival techniques, they were able to correlate the emission of X-rays with the stepping process. Howard et al. (2008) and Biagi et al. (2010) solidified the idea that burst of X-rays are emitted during the stepping process of negative leaders. Biagi et al. (2010) did so by using simultaneous observations with high-speed video, and measurements of current, field changes, and X-ray emissions. The work done at ICLRT showed that all types of subsequent stroke leaders (in rocket-triggered lightning) emit X-rays, including dart, dart-stepped, and "chaotic" dart leaders (Hill et al., 2012). Particularly, chaotic dart leaders (which are characterized by numerous, narrow, irregular pulses in the electric field derivative signal) seem to be more prolific X-ray emitters than the other two kinds (Hill et al., 2012).

Saleh et al. (2009) compared multi-station measurements of X-ray emissions made with the Thunderstorm Energetic Radiation Array (TERA) at the ICLRT with Monte Carlo simulations of runaway electron propagation, their collisions with air molecules, and the subsequent Bremsstrahlung X-ray emissions. Saleh et al. (2009) reported that the energetic electrons that emit X-rays can have a characteristic energy of about 1 MeV, which is not consistent with the relativistic runaway electron avalanche mechanism (RREA) (Gurevich et al., 1992), which predicts that the runaway electrons should have a characteristic energy of 7.3 MeV. Schaal et al. (2012) expanded on the work of Saleh et al. (2009) and compared measurements of spatial and energy distributions of X-ray emissions made with TERA at the ICLRT with Monte Carlo simulations. Through this comparison Schaal et al. (2012) showed that the characteristic energy electrons responsible for X-ray emissions in lightning leaders is less than 3 MeV. Once again in contrast to the 7.3 MeV value predicted by the RREA theory. Schaal et al. (2012) also reported that electron luminosity increases exponentially with the return stroke current up to about 10 kA.

Arabshahi et al. (2015) performed measurements of the X-ray energy spectrum of rocket-triggered lightning by developing an X-ray spectrometer. The Atmospheric Radiation Imagery and Spectroscopy spectrometer (ARIS-S) is made of seven NaI(Tl) scintillators coupled with PMTs. These detectors are all located next to each other and have variable shielding around them, consisting of varying thicknesses of steel and lead, which constrain the energy range of photons that can be stopped by a particular channel. The combination of the multi-channel measurements with Monte Carlo simulations allowed the authors to determine that the spectrum of X- and gamma-rays emitted by rocket-triggered lightning follows an inverse power-law distribution $\propto \varepsilon^{-\lambda}$, where ε is the energy of an individual photon, and the power-law exponent λ varies between 2.45 and 2.92 for a particular type of leader and for the entire data set (Arabshahi et al., 2015).

The studies reviewed above support the idea that RREA do not play a significant role in the production of runaway electron fluxes emitted by leader steps. In lightning leaders, the so-called thermal (or cold) runaway mechanism seems to be a better candidate to explain acceleration of electrons into the runaway mode (Dwyer, 2004; Moss et al., 2006; Celestin et al., 2015). This mechanism requires the electrical discharge to produce electric fields in excess of 30 MV/m, ten times higher than the conventional breakdown threshold, for electrons to overcome the friction force experienced by collisions with air molecules. d'Angelo (1987) suggested that these high fields could be present at the streamer heads, leader tips, or even in the lower-density leader channel. Most TERA sensors include detectors with NaI(Tl) scintillating crystals and suffer from pile-up issues. However, Schaal et al.'s data set included one natural flash detected by two $LaBr_3$(Ce) detectors, which have a much shorter decay time. Since $LaBr_3$(Ce) is not as subject to photon pile-up issues, this allowed the authors to estimate the X-ray single-photon energy spectrum. Xu et al. (2017) used this data set as ground truth for their Monte Carlo simulations, and showed that the measured X-ray spectrum of Schaal et al.'s flash is fully consistent with the thermal runaway acceleration mechanism, for a leader with 10 MV potential difference between its tip and the surrounding environment.

Mallick et al. (2012) reported X-ray emissions associated with leaders of natural cloud-to-ground lightning and showed that, in some cases, subsequent strokes can emit more X-rays than the leaders preceding the first return stroke in the same flash. These authors attributed this effect to the reduced air density inside of the (warm) decaying return stroke channel, which would allow the electric field enhancement created by the dart leader to accelerate electrons in an environment with reduced collisional rates, i.e., reduced friction force (see also, Tran et al., 2019). Mallick et al. (2012) also reported that, for strokes within 2 km of their observation facility, X-ray emissions were associated with 88% of first-stroke and 47% of subsequent-stroke leaders (see also, Kereszy, 2021, Figure 3-11).

The aforementioned references established that the energy spectrum of X- and gamma-rays emitted by lightning leaders is softer than what is predicted by the RREA theory. The RREA theory (augmented by relativistic feedback mechanisms), nonetheless, successfully explains the spectra of Terrestrial Gamma-ray Flashes (TGFs), emitted upward by thunderclouds and registered at satellite altitudes (Dwyer & Smith, 2005; Dwyer, 2008). The story becomes more complicated when we consider downward TGFs, particularly the ones timed to the downward leader propagation, which are observed at the Utah Telescope Array (TA) (Abbasi et al., 2018, 2023; Belz et al., 2020). The TA downward TGFs seem to have a harder spectrum than leader X-rays, but at the same time, weaker fluence than upward TGFs. In the words of Smith et al. (2018), the existence of the TA TGFs blurs the clear-cut distinction between leader X-rays (soft, weak) and TGFs (hard, strong).

Measurements of X-rays emitted by natural lightning are quite important for pinning down their source mechanisms and the role of runaway electrons in leader physics. However, spectral information on the X-rays emitted by natural lightning are still scant in the literature, since the vast majority of data acquired at the ICLRT correspond to rocket-triggered lightning and/or it was collected with NaI(Tl) detectors. To the best of our knowledge, there is only one (other) report of a direct measurement of the energy spectrum of X-rays emitted by a natural lightning flash, and it is the single-stroke flash MSE 10-01 in Schaal et al. (2012, Figure 10). By "direct", we mean without contamination of photon pile-up, and not indirectly determined via Monte Carlo simulation. The present paper is aimed at augmenting the data available on the energy spectrum of X- and gamma-rays emitted by natural lightning. We report on the composite spectra of four natural flashes recorded in the Summer of 2022 at Langmuir Lab with a fast $LaBr_3$(Ce) detector. We confirm the spectral dependence previously reported in the literature and show that stepped leaders have a harder spectrum than dart leaders.

2 Methods

Over two decades after the original discovery, Langmuir Lab's mountain-top facility (Figure 1) remains an ideal place to perform X-ray observations of natural lightning due to three main reasons: (i) orographic effects facilitate the formation of single-cell convective thunderstorms over the lab during the yearly monsoon season, (ii) at 3.3 km above mean sea level, the lower air density reduces photon attenuation, and (iii) Langmuir Lab has an extensive list of co-located atmospheric electricity instruments that provide better context on the production of runaway electrons. The main instrument — the X-ray instrument box — was deployed atop of an underground Faraday cage room (called Kiva, Figure 1a) located on South Baldy peak, the highest peak in the Magdalena Mountains in central New Mexico. This is the exact same location where Moore et al.'s detectors were located. Figure 1c shows South Baldy peak as viewed from the Langmuir Lab main facility, which is located 1.8 km away. Below we present the instrumentation and methods used in this study.

2.1 Sensors

A key feature of the present investigation is the use of a fast data acquisition system (DAS). The DAS used is similar to the one used by Akita et al. (2014) and subsequent lightning interferometry works (Rison et al., 2016; Jensen et al., 2021), and it operated at a 180 MHz sampling rate. This DAS was housed inside of the Kiva and linked to the same slow electric field antenna Moore et al. (2001) used to trigger their experimental setup. This slow antenna has a time constant of 31 ms and triggered data acquisition when the electric field change reached 2.5 kV/m. Four sensors were connected to our DAS:

LaBr A $2'' \times 2''$ $LaBr_3(Ce)$ scintillation detector (hereafter simply referred to as LaBr) manufactured by Saint-Gobain was mounted in our instrument box on top of the Kiva (Figure 1b) to detect the X-ray emissions. The LaBr crystal has a fast decay time of 16 ns, which results in a narrow voltage pulse recorded in the DAS (<100 ns). The pulse has rise/decay times of 16/54 ns. The background radiation rate during storm time for the LaBr was measured to be 1 photon per 3 ms.

NaI The X-ray instrument box also contained a $2'' \times 2''$ NaI(Tl) scintillation detector (hereafter NaI for short). This detector was included for the sake of presenting a comparison between the two types of detectors used in this research area. This particular NaI unit is connected to a pulse-shaping amplifier, making the registered voltage pulse have a duration of >10 μs. This is the result of a design choice made in our group for a previous research project. This was needed to allow for the operation of NaI detectors with 100 kHz data acquisition systems. All key results of this paper are based on the LaBr detector measurements, and the NaI data is just shown for comparison. The background radiation rate during storm time for the NaI detector was measured to be 1 photon every 20 ms.

Fast antenna A fast electric field change antenna (FA) with a time constant of 100 μs and a flat bandpass (between 20 kHz and 70 MHz) was used to measure rapid field changes from lightning leaders. The FA uses the standard "inverted salad bowl" design and it sits on top of the Kiva, essentially co-located with the X-ray sensors (Figure 1a).

Timing A microsecond resolution GPS unit (Figure 1b) was used to time the the recordings of the three instruments described above. This allowed for synchronization of our measurements with other instruments located at Langmuir Lab and with the Earth Networks Total Lightning Detection Network (ENTLN) data.

We used the following supporting instruments and data sets to characterize the flashes analyzed in this paper:

Slow antenna As mentioned above, an insensitive slow antenna with time constant of 31 ms was used to trigger the DAS. It has the same antenna design as the one used in Moore et al. (2001) and it was sampled at 250 kHz.

LEFA A single station from the Langmuir Lab's Lightning Electric Field Array (LEFA) (Lapierre et al., 2014; Contreras-Vidal et al., 2021) was used in this study. LEFA is characterized by its ultra-slow time constant (3 s) and high dynamic range (consisting of three different gain levels). LEFA provided us with additional information to distinguish between dart and stepped leaders, particularly when the FA saturates. LEFA recordings were digitized at 50 kHz.

Field mill A field mill recording at 10 Hz was used in this analysis. Field mills are capable of capturing the slow field changes associated with the overall storm electrification and subsequent dissipation (Christian et al., 1980).

THOR One of the units of the Terrestrial High-energy Observations of Radiation (THOR) instrument (Smith et al., 2019) was deployed at Langmuir Lab during the Summer of 2022. THOR is located at the main lab, 1.8 km away from our X-ray sensor. THOR did not record energetic emissions associated with any of the flashes analyzed in this paper. This fact is briefly used later to constrain the footprint size of the X-ray emissions.

ENTLN We used the Earth Networks Total Lightning Detection Network (ENTLN) data to assist us with flash classification (cloud-to-ground versus intracloud), as well as determining stroke order. More importantly, ENTLN provided the flash peak current and location (i.e., distance to the X-ray sensor).

We used 4 electric field antennas to give proper flash context and be able to "see" field changes from fast to very slow lightning and storm processes. In order of increasing time constant we had: the fast antenna, slow antenna, LEFA, and the field mill. The

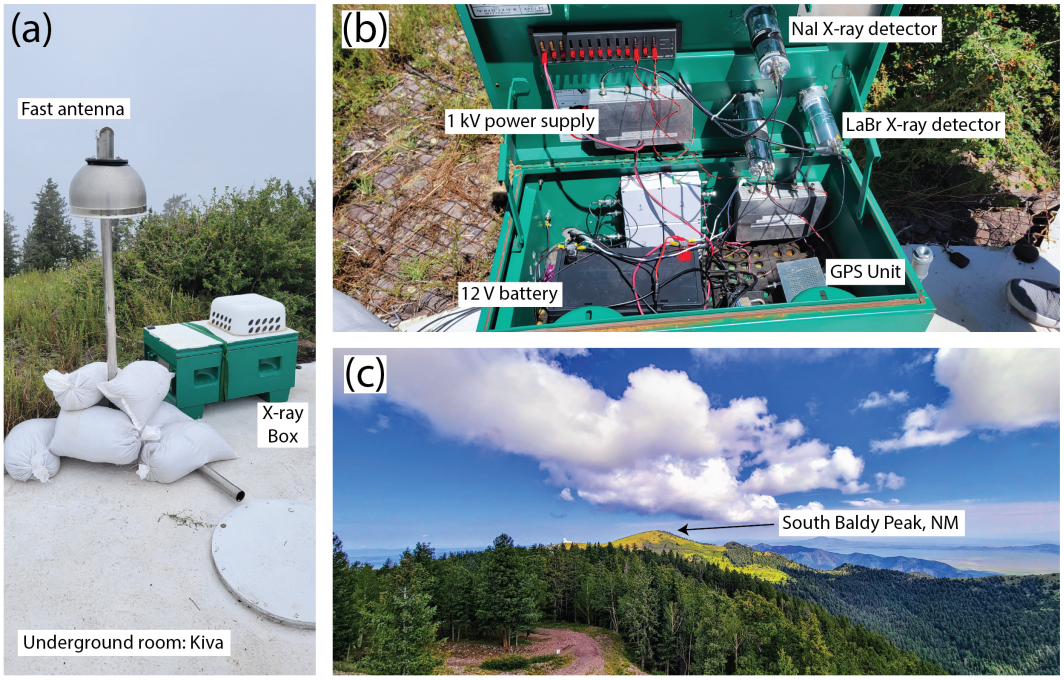

Figure 1. Instruments & deployment. (a) X-ray box and fast electric field antenna on top of the Kiva underground Faraday cage room (which houses the 180 MHz data acquisition system). (b) X-ray box contents: LaBr and NaI X-ray detectors, power source, and the GPS unit. (c) The Kiva sits atop South Baldy Peak in the Magdalena Mountains photographed from the Langmuir Lab main facility. Not shown are Langmuir's slow antenna and (non-collocated) LEFA.

slow antenna and field mills have been used in our group for many years and have been properly calibrated. The calibration includes determining the gain factor associated with placing the antenna on a stand 1 m above ground level and also with deploying it in a mountainous terrain. For this study LEFA and the FA were not directly calibrated. In order to display them in the same plot as the slow antenna we have empirically determined the calibration factors by ensuring that they (FA and LEFA) predict the same field changes as the slow antenna. Therefore, we only report quantitative field changes measured by the slow antenna. For the other two antennas, qualitative field change features are used to discern between dart and stepped leaders.

2.2 X-ray detector calibration

Standard radioactive sources were selected to calibrate and test the linear response of the LaBr and NaI detectors. Figure 2a and 2b show data from the five sources used (Ba-133, Na-22, Cs-137, Zn-65, Co-60) and the linear response of each detector. All sources were placed 10 cm above the detector. Figures 2a & 2b show that both detectors have a linear response in the range of interest. In a separate study, the linearity of the LaBr detector was verified down to 20 keV (Contreras-Vidal et al., 2022).

The two detectors were powered with the same power supply at 1 kV, which defined their gain. As a consequence, the maximum energy that each detector was able to record was 6 and 1 MeV, for the LaBr and NaI, respectively. The PMT gain can be influenced by the external temperature. In order to check if this may introduce large errors, we collected data wit the Na-22 source at the field during a hot Summer day (during deployment). Figure 2 shows that the data collected in the field (red symbols) agrees

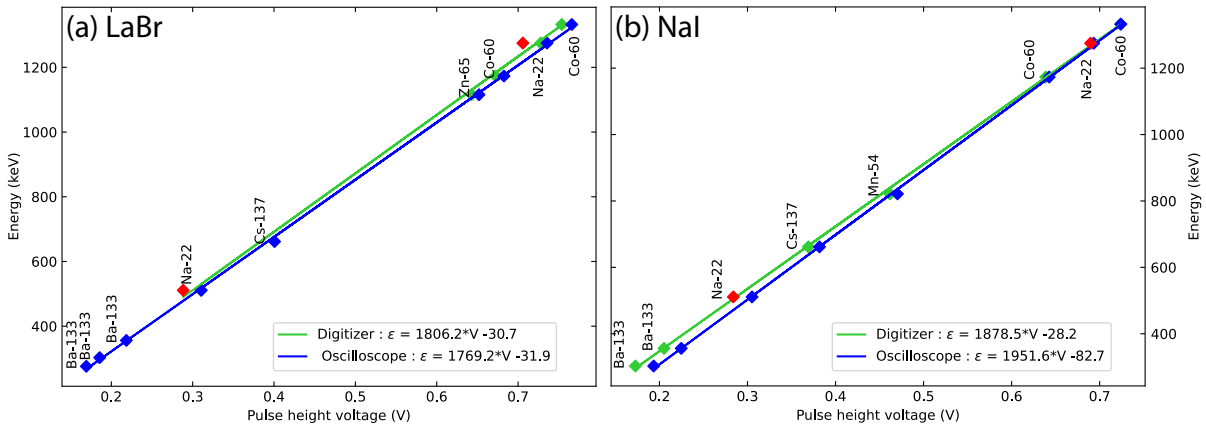

Figure 2. Calibration of the X-ray detectors using 5 different standard radioactive sources. Panels (a) and (b) show the linear response of the Labr and NaI detectors, respectively. The green line corresponds to the response of the detectors using our DAS, while the blue line corresponds to the response of the detectors using a LeCroy HDO6014a oscilloscope (same as in Contreras-Vidal et al., 2022). The red symbols correspond to data collection with the DAS at the field site.

well with the data collected in the lab (green symbols). The figure also shows that both also agree well with data collected using a different acquisition method (a standard oscilloscope, shown as blue symbols). Since the agreement has been deemed good, no correction for temperature has been added to the voltage-to-energy conversion formula (listed in the figure legend).

2.3 Photon pile-up resolution

Figure 3a shows an X-ray burst from event A1 (discussed later). Pile-up can be seen in the form of the characteristic X-ray pulse shapes being interrupted by incoming photons arriving within the pulse duration, less than 100 ns apart. In this work we are able to resolve photon pile-up due to three main reasons: (i) we employ a fast scintillator, which has a crystal with short decay time, of 16 ns, (ii) we collect data at a high-sampling rate of 180 MHz, corresponding to 5.56 ns between samples, and (iii) the recorded flashes took place at a typical distance of 500 m from the LaBr detector. The latter effect reduces pile-up because Compton scattering will tend to spread the photons in a given burst spatially and, as a consequence, temporarily. Photon pile-up is a major issue in the interpretation of laboratory measurements due to the compactness of the spatial scales involved, of the order of 10s of centimeters (Contreras-Vidal et al., 2022; da Silva et al., 2017; Pantuso et al., 2022). This issue is also present in the measurements of rocket-triggered lightning X-rays, where detectors are 10s of meters away from the source (Saleh et al., 2009; Schaal et al., 2012). However, factor (iii) alone alleviates this issue substantially as the distance between source and detector increases to 100s of meters.

Data from the LaBr detector calibration provided a wealth of characteristic X-ray pulse shapes. An analytical expression was obtained for the X-ray pulse shape by normalizing a synthesis of fifty X-ray pulses from calibration data and fitting them with a closed-form function. This is the impulse response of the LaBr to a single photon, and it was best fit by a skewed Gaussian function. These fits lined up with our characteristic X-ray pulse on the order of $R^2 \geq 0.999$. Once this analytical fit was obtained, only the height and location of the pulse needed to be adjusted to match the recorded traces.

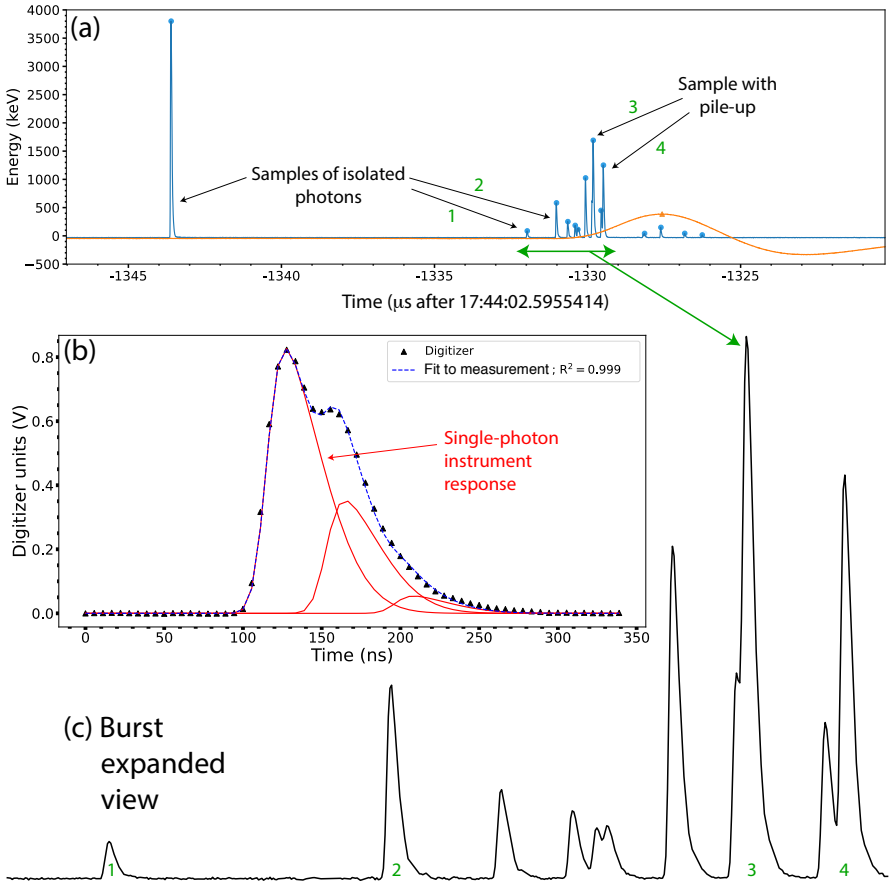

Figure 3. (a) A 20-μs X-ray burst from event A1. The recorded voltage traces for the LaBr and NaI detectors are shown in blue and orange, respectively. (b) An example of photon pile-up occurrence and our strategy to resolve it. This particular pulse did not occurred during the burst shown in panel (a). Panel (b) shows that photon pile-up can be resolved if photons arrive more than 16-ns apart by fitting the recorded waveform with several single-photon impulse responses (with different arrival times and amplitudes). (c) Expanded view of the LaBr X-ray burst with sample photons labelled.

Occurrences of photon pile-up were manually isolated by locating irregular X-ray pulse shapes in the LaBr detector channel. X-ray pulses derived from our analytic fit were then placed nearby the pileup event, at which point their locations and magnitudes would be adjusted until their collective sum fitted the piled-up event with a coefficient of determination no less than 0.97. A plot of one such pile-up resolution process is shown in Figure 3b. The solid red curves correspond to the single-photon impulse response, with the digitizer data shown as black triangular markers. The dashed, blue line is the sum of all red pulses, fitting the digitizer data with $R^2 = 0.999$. After analyzing all data reported in this paper, which consists of hundreds of X-ray pulses correlated to lightning activity, we found that pile-up occurred in only 12 % of all recordings. The remaining 88 % are perfectly fit by the single-photon impulse response. Tests with the fitting procedure shown in Figure 3b revealed that if two photons arrive within the decay time of the crystal (=16 ns or four samples), the system is not able to resolve the two photons.

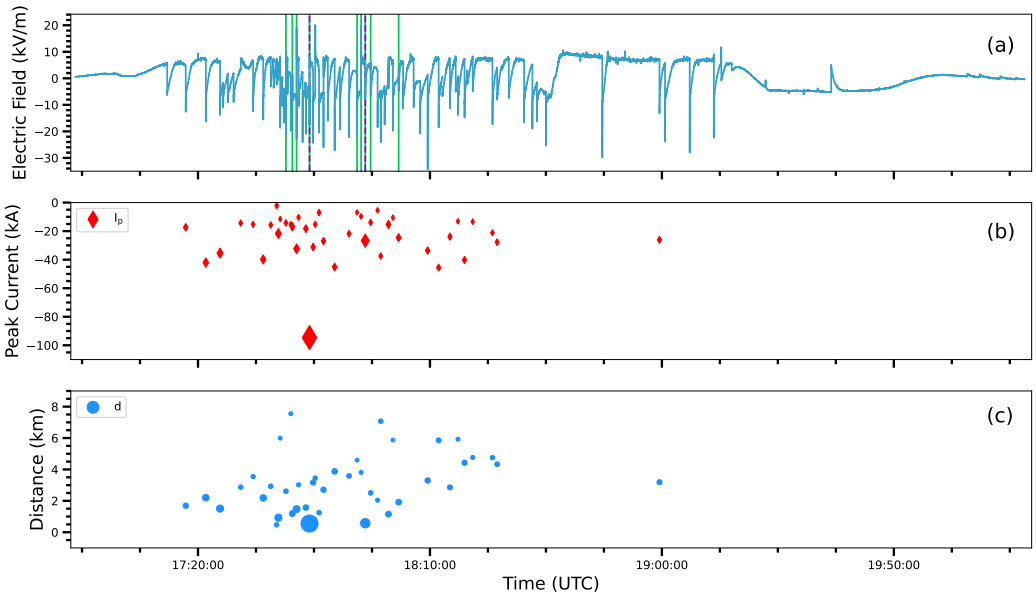

Figure 4. An overview of the observed thunderstorm on August 9, 2022, lasting from approximately 17:00 to 20:00 UTC. (a) Information from Langmuir's electric field mill spanning the whole storm. Vertical lines indicate lightning flash that triggered our system, with purple lines indicating triggers with X-ray observations. (b) A display of peak return stroke current for individual −CG flashes within 10 km of South Baldy peak. (c) Flash distance to the X-ray detectors, as reported by ENTLN. In panels (b) and (c) markers are sized according to the ratio of peak current to distance, which makes the two events with X-ray detections stand out.

3 Results

Our most interesting recordings took place during a midday thunderstorm on August 9, 2022. This storm lasted approximately three hours between 17:00 and 20:00 UTC (11 AM to 2 PM local time), as shown in Figure 4. Figure 4a shows the measured electric field through the storm as seen by an electric field mill. The storm's main stage has a positive electric field (i.e., directed upward) due to the dominant effect of negative charge overhead. This is indicative of a normally-electrified storm. The numerous negative deflections (or dips) in the field mill record are negative cloud-to-ground lightning flashes (−CGs). At the end of the record we can see a characteristic end-of-storm oscillation in the electric field (Moore & Vonnegut, 1977).

The nine vertical lines indicate flashes that triggered the DAS, with the two purple lines indicating triggers containing X-ray detections. These flashes were correlated with ENTLN data to obtain their peak current, classification, and distance from the Kiva for each individual stroke in a flash (Zhu et al., 2017). Figure 4b shows the peak current for all −CG flashes within 10 km of the X-ray detectors. Figure 4c shows the actual distance between these lightning flashes and the X-ray detectors. As discussed by Mallick et al. (2012), the probability of detecting X-rays from lightning increases with peak current (I_p) and decreases with distance (d). Therefore, we can speculate that the probability of detecting X-rays should increase with the following ratio: I_p/d. The size of markers in Figures 4b–4c are scaled according to the I_p/d ratio, and we can clearly see that the two flashes containing X-ray emissions stand out, particularly the first one. The ratio I_p/d is proportional to the measured field change, which is also a proxy for the

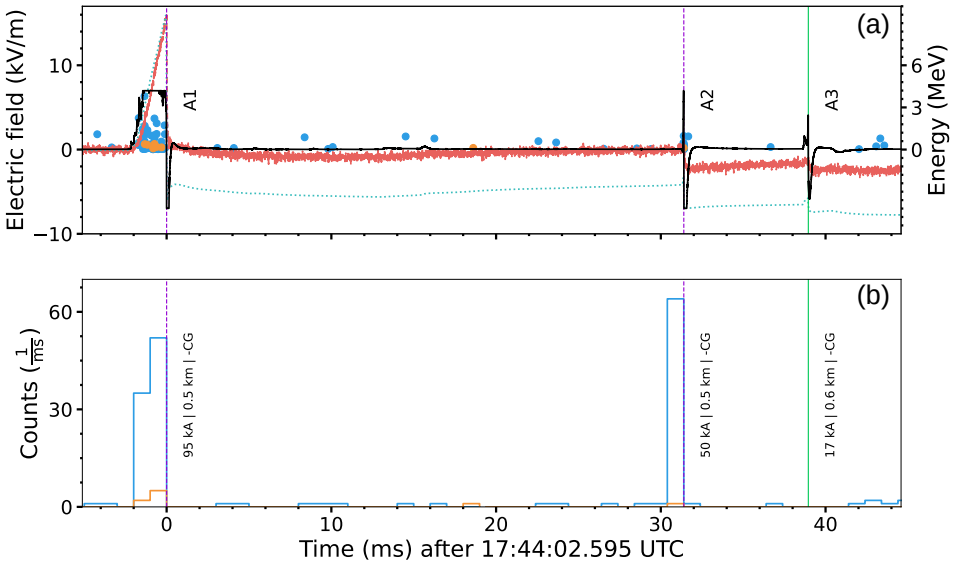

Figure 5. The first three return strokes in flash A on a scale of tens of milliseconds. (a) Data from electric field antennas and X-ray detectors. The three traces correspond to the slow antenna (red), LEFA (dotted teal curve), and fast antenna (black). X-ray energy pulse peak locations are shown as blue (LaBr detector) and orange (NaI) dots. (b) Histogram showing photon counts in a one-millisecond window by the LaBr (blue) and NaI (orange) detectors. For return strokes with associated X-ray observations, all photons were detected during the preceding leader phase.

probability of detecting X-rays. We note that the $1/d$ scaling is not the precise trend for deposited X-ray energy versus distance. According to Saleh et al. (2009), this trend is actually $\propto \exp(-d/120\,\mathrm{m})/d$, with the additional decaying exponential term arising from X-ray absorption and scattering in air.

Figure 5 shows a zoom on the order of tens of milliseconds of the first lightning flash containing X-rays and its individual return strokes. This flash took place at 17:44:02.6 UTC and it is referred hereafter as flash "A". Each individual return stroke reported by ENTLN, including the one that triggered the system, are represented as vertical lines. In a similar fashion as Figure 4a, return strokes of leaders with X-ray observations are marked by dashed, purple lines, with all other strokes marked with solid, green lines. Included with each return stroke are reported ENTLN data, such as classification (IC vs. CG), peak current, and distance to the X-ray detectors. This lightning flash was composed of five return strokes (events A1 to A5). Only the leaders associated with the first (event A1, a stepped leader) and second (event A2, a dart leader) strokes produced detectable X-rays. Both events A1 and A2 lead to return strokes with high peak currents of 95 and 50 kA, respectively. As shown previously in Figure 4, flash A clearly stands out as having the highest peak current of the entire storm and by taking place very close to our detectors.

In Figure 5a, the recorded electric field changes are shown alongside the X-ray energy measurements. The slow antenna is shown as a red dashed line, LEFA as a teal-dotted line, while the fast antenna is overlaid as a solid, black curve. During this campaign, the FA was designed to provide accurate electric field readings up to 7 kV/m before saturation. This figure is given in scaled units, as discussed in Section 2.1. Satura-

tion in the fast antenna can be seen in events A1 and A2 in Figure 5a, but not A3. In conditions where the fast antenna saturates we rely on the additional information provided by the other two antennas. Looking at the electric field records it is often pretty easy to tell stepped and dart leaders apart. Stepped leaders display this characteristic ramp in the electric field change prior to the return stroke dip, which lasts on the order of milliseconds, and is associated with the downward motion of the stepped-leader network (see event A1).

The dots in Figure 5a show the energy of detected X- and gamma-ray photons, with the LaBr (blue) and NaI (orange) detectors. The ordinate of each dot represents its energy with values indicated on the right-hand side vertical axis. The histogram in Figure 5b correspond to the number of photons observed by each detector in a one-millisecond time window, using the same color scheme as in Figure 5a. It is clear that events A1 and A2 had photon counts much higher than the background rate of the LaBr detector (1 photon every 3 ms). Event A1 had 87 photons associated with it, detected during the stepped leader descent. The average energy of the detected photons was 416 keV and the maximum energy was 3.8 MeV (well into the gamma range). Event A2 had 64 photons detected during the dart leader descent, with an average energy of 138 keV and a maximum of 969 keV.

Figure 6 has a similar format to Figure 5 with the key difference being that we display a zoom, of the order of milliseconds, into event A1 to show the X-ray detections in greater detail. Figure 6a includes again electric field information from the fast antenna, but omits data from the other two antennas for the sake of clarity. X-ray peak locations are included, as well as the full trace of each X-ray detector channel. Figures 6b and 6c show histograms of photon counts by each detector binned in 100- and 10-μs windows, respectively. A brief glance at Figure 6b would indicate that the X-ray emissions are continuous and last for 1.5 ms. The higher temporal resolution of Figure 6c reveals that X-ray photons come in bursts. Our interpretation of these results is that, in alignment with previously-published work, these bursts are associated with leader steps. Nonetheless, attempts to align the bursts in Figure 6c with features in the LEFA recording (which did not saturate) did not yield a straightforward correlation. This is likely due to the fact that there must be a multitude of leader tips stepping towards the ground at any given time (see e.g., Urbani et al., 2021). The photon burst highlighted in Figures 3a and 3c is an excerpt of this event and took place 1.33 ms before the return stroke. A comparison between the NaI and LaBr data reveals that the fewer NaI detections correlate with stronger bursts seen in the LaBr detector (Figures 6b–6c). This lends further credence to the conclusion that the X-rays from stepped leaders come in bursts. Hereafter, we shall focus the discussion on the LaBr data, and the NaI detections will be shown simply for the sake of completeness. Figure 6 makes the obvious case that the LaBr detector can reveal so much more details about the source.

Figure 7 shows a zoom on the order of tens of microseconds into event A2, a dart leader followed by a subsequent return stroke. An immediate noteworthy observation of this event is that all the X-ray emissions of this event occurred on a comparable time scale of one single burst of event A1. The stepped leader produce 87 (detectable) photons in 1.7 ms, while the dart leader produced 64 photons in under 25 μs. It seems that the dart leader X-ray emission process behaved as a single, very-intense stepped leader step. Figure 7a shows that the field change associated with a descending dart leader also ramps up from zero prior the return stroke. But the key difference is that this process is much faster than in a stepped leader, of the order of tens of microseconds.

We zoom even further into the X-ray pulses and catalog the energies of all individual photons that were recorded in the LaBr detector. As discussed in Section 2.3, we are able to distinguish individual photons to a 16-ns temporal resolution. The same process was repeated for other 3 flashes of the 2022 monsoon season where X-rays were observed. They are referred to as flashes B, C, and D in the Appendices. The LaBr detector reg-

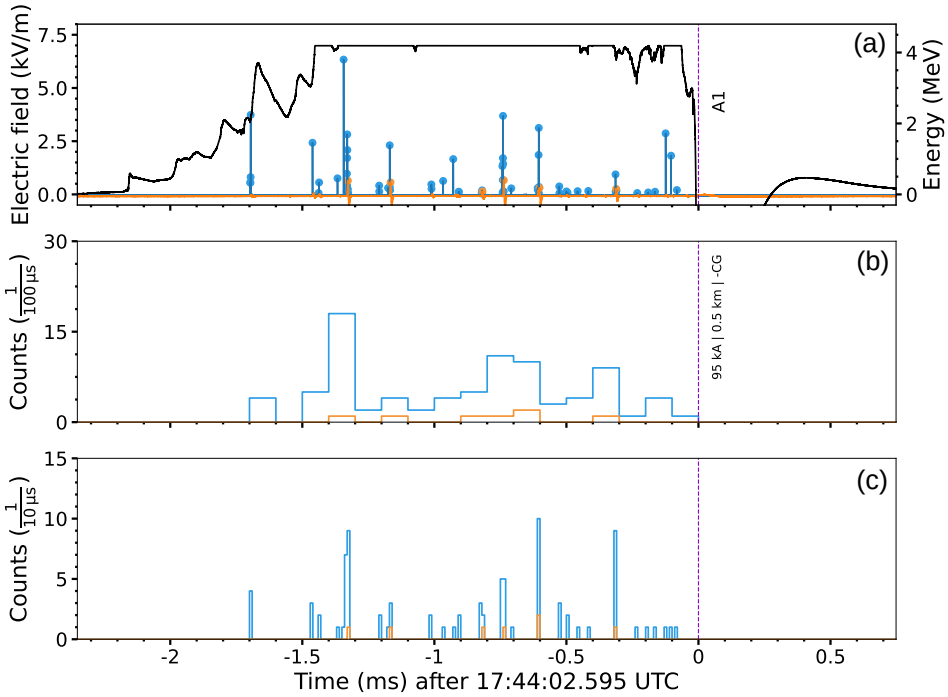

Figure 6. A zoom into event A1, the first return stroke and preceding stepped leader from Figure 5, on a scale of a few ms. (a) Electric field measured with the fast antenna (on the left-hand side axis), plotted alongside the X-ray detections (full trace and peaks with values displayed on the right axis). (b-c) Histogram showing photon counts in 100- and 10-μs windows. Across the three panels, data for the LaBr and NaI detectors are displayed in blue and orange colors, respectively.

istered a total of 127 and 120 photons associated with stepped and dart leaders, respectively, across these four flashes. The median energy of photons emitted by stepped leaders is 115 keV, while their maximum value is 3.8 MeV. Meanwhile, photons emitted by dart leaders had a median energy of 65 keV and a maximum of 1.16 MeV. A summary of each event's number of photons, maximum energies, peak electric fields, and ENTLN stroke information is provided in Table A1 in Appendix A.

Figure 8 shows the measured X- and gamma-ray spectrum. The top row shows data for flash A discussed in detailed in this Results section, while the bottom row shows composite spectra for the four flashes recorded in the Summer of 2022. The spectra shown in the four panels follows a power-law distribution, $\propto \varepsilon^{-\lambda}$, in agreement with Arabshahi et al. (2015), with varying values of the exponent λ. The power-law index was determined in the four plots by fitting the closed-form dependence to the data, yielding fits with $R^2 > 0.88$. The inferred λ values are listed in the figure legends. A comparison between the spectra of stepped (Figures 8a,8c) and dart (8b,8d) leaders reveals that, although both spectra are similar, dart leaders have a softer spectrum with a much lower population of >1 MeV photons. The power-law index for stepped leaders is $\lambda = 1.21$, while for dart leaders it is $\lambda = 1.96$. Note that a smaller value of λ corresponds to a distribution with a longer tail. For different types of dart leaders in rocket-triggered lightning, Arabshahi et al. (2015) reported $\lambda = 2.45$–2.53, which is 25–29% larger than the value reported here. This means

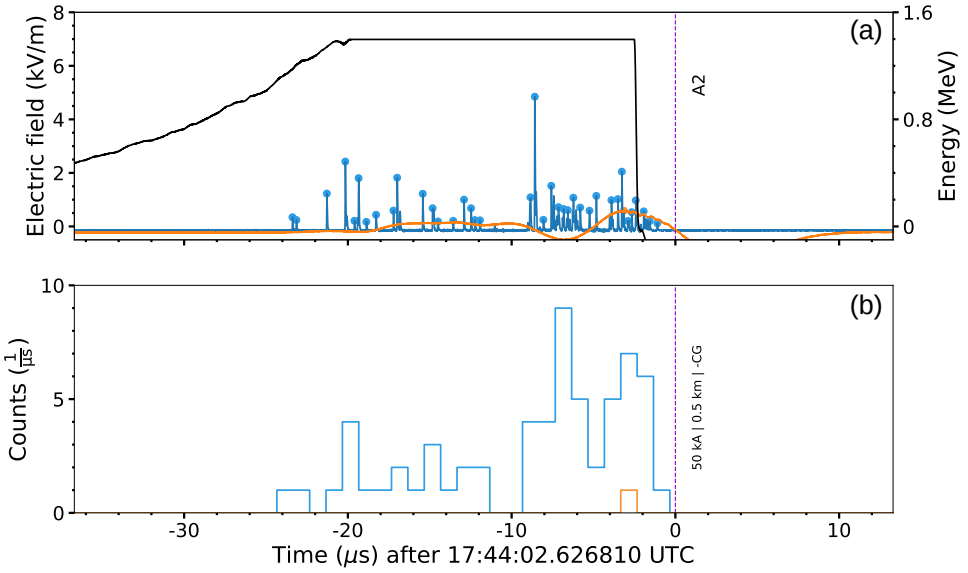

Figure 7. A zoom into event A2 from Figure 5, a dart leader followed by a subsequent return stroke, on a scale of tens of microseconds. The figure format is the same as in Figure 6, with the only difference that the histogram in panel (b) is binned in 1-μs windows.

that, contrasting these two particular data sets, we can say that the energy spectra of (natural) dart leaders recorded at Langmuir Lab is (somewhat) harder than in rocket-triggered lightning at ICLRT. It should be noted that the composite spectra (Figures 8c–8d) are dominated by events A1 and A2 (8a–8b). These events contributed to over 60% of the detected photons. Nonetheless, there is a measurable difference in the power-law index between flash A versus the entire data set, with the latter producing 5–10% larger λ values.

Mallick et al. (2012) reported that in some cases a dart leader (leading to a subsequent stroke) in a flash can produce more X-rays than the first-stroke (stepped) leader. These authors argue that the reduced air density in the (pre) dart-leader channel may facilitate runaway electron acceleration. Our observations reveal that the picture may be far more complex than that, i.e., that the X-ray emission process is profoundly different between stepped and dart leaders. We make this statement based on the vastly different temporal patterns reported in Figures 6 and 7, as well as, on the different spectral hardness in Figures 8a and 8b. The stepped leader emits X-rays over a long time period, of $\gtrsim$1 ms, while the dart leader X-rays come within $\sim$25 μs. Despite the distinctly different durations, the amount of X-ray photons detected is similar. The stepped leader produced more photons, but just 36% more. In just one of the four flashes reported in this paper (in the Appendices), the X-ray count in a dart leader superseded the stepped leader.

We interpret our findings as indicative of two key differences between stepped- and dart-leader X-ray emissions. First, the stepped leader photon spectra is harder because it is able to accelerate electrons to higher energies. This likely happens because the electric fields at the tips of advancing stepped leaders are higher than in dart leaders, since the former needs to break down virgin air to propagate. Perhaps even the impulsive nature of the stepping process facilitates acceleration. Second, dart leaders are somewhat

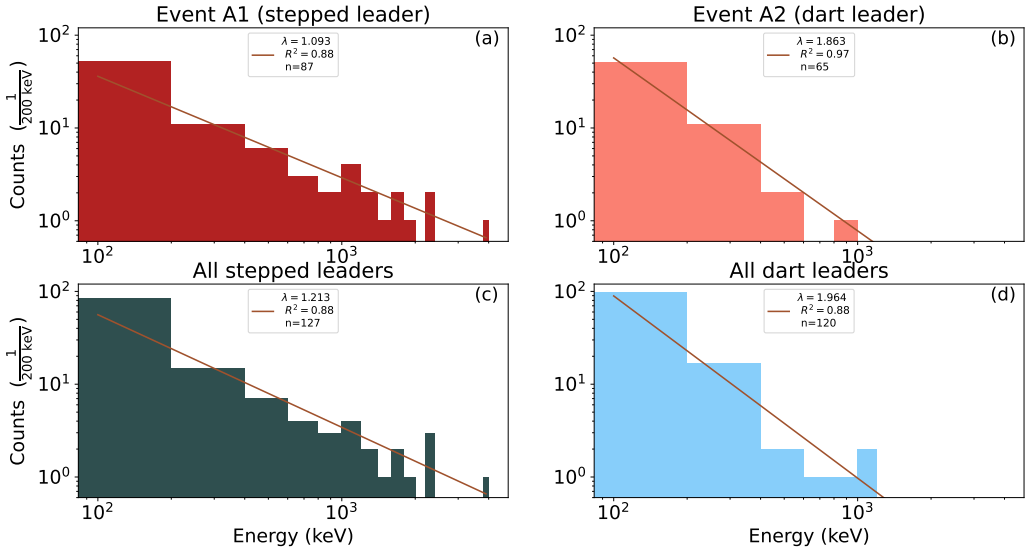

Figure 8. Energy spectra of X- and gamma-ray photons emitted by natural lightning, for flash A only (a-b), and for the entire data set (c-d). The left- and right-hand side panels show data for stepped and dart leaders, respectively. Across the four panels, experimentally-determined spectra, binned in 200 keV bins, is compared to power-law distribution fits.

more efficient X-ray producers. They are able to emit a comparable amount of X-rays in a substantially-shorter time window. A significant portion of the asymmetry in the emission's temporal profile can be explained from the fact that dart leaders are roughly ten times faster than stepped leaders (da Silva et al., 2023; Jensen et al., 2021).

The photon energy spectra of stepped leaders extends well into the gamma range. This helps fuel the idea that there may not be a clear cut distinction between leader X-rays and downward TGFs (particularly the downward TGFs that take place during leader propagation, such as the ones observed at the Utah Telescope Array). It may be that if the potential drop between leader tip and environment is just large enough to accelerate runaway electrons (e.g., a few MV), the X-ray emissions display a soft power-law spectrum. This is the case of our dart-leader detections. If we increase the potential drop, we start measuring a harder power-law spectrum, such as we see in the stepped-leader recordings. If the potential becomes becomes very large (in the 100s of MV), the field around the leader tip may be able to sustain avalanching, and the photon spectra will have the characteristic RREA shape (Celestin et al., 2015).

We conclude the discussion by noting that the footprint of the X-ray emissions detected at Langmuir Lab is no larger than 2 km wide (or 1 km radius). We have reached this conclusion based on two facts. First, no detections were made for lightning flashes that happened more than 0.6 km away from the sensors. The August 9 storm contained additional triggers, all marked as vertical lines in Figure 4. Triggers corresponding to flashes that took place more than 1.2 km away from the sensor did not contain X-ray emissions. Flash-to-sensor distance was estimated using ENTLN data, which reported semi-major ellipse errors of 100–200 m. Second, the UCSC THOR instrument was located 1.8 km (roughly) South of our X-ray sensors. THOR did not register any concurrent surges in X-ray emissions associated with the four lightning flashes presented in this paper. The estimated size of the X-ray emission footprint lays in between the ICLRT triggered dart-leader X-rays (of <1 km in diameter in Schaal et al., 2012) and the Utah TA downward TGFs (of <5 km in diameter in Abbasi et al., 2018).

4 Summary and conclusions

In this article, we described in detail a natural lightning flash and its X- and gamma-ray emissions. This flash was detected by two X-ray instruments, including a fast LaBr scintillator connected to a 180 MHz digitizer, as well as four electric field-sensing antennas. These four antennas can probe a multitude of time scales, revealing contextual details of the storm, its flashes, and their individual leaders. In this flash, the X-ray emission associated with the first-stroke, stepped leader lasted 1.7 ms and came in multiple bursts, meanwhile the X-ray emissions associated with the subsequent stroke leader (a dart leader) lasted only 25 μs. Despite the shorter duration, the dart leader managed to produce a comparable amount of X-rays. This is in alignment with the findings of Mallick et al. (2012), who found that in some flashes a subsequent stroke leader may produce more X-rays than the first-stroke one. We have one case, presented in the Appendices, that behaved in a similar manner.

Furthermore, we reported the composite energy spectra of four lightning flashes recorded in the Summer of 2022 at Langmuir Lab, and discriminated them according to the type of leader: stepped (4 cases) versus dart (7 cases). Our results show that X-ray emissions associated with both stepped and dart leaders follow an inverse power-law distribution, and contain no significant evidence of RREA contribution. This in agreement with previous work by Arabshahi et al. (2015) and Xu et al. (2017). We also determined that the energy spectra of stepped leaders seem to be harder than dart leaders, i.e., containing more gamma (>1 MeV) photons, and displaying a longer tail. We interpret these findings as a consequence of the fact that electric fields at the tips of stepped leaders must be stronger than in dart leaders, since the former needs to break down virgin air to propagate. One may speculate that if a particular stepped leader has a very high potential drop with respect to the environment, RREA may take place around the leader tip, and bring the fluence to the high levels associated with TGFs.

Since our conclusions regarding the spectral characteristics of leader X-rays are based on just 4 flashes, we must deem these results preliminary, and must plan to continue with the experimental campaigns to collect more data. Future work may include correlating X-ray emissions with three-dimensional flash structure, as revealed by the Lightning Mapping Array (da Silva et al., 2023), or by broadband interferometry (Jensen et al., 2021; Urbani et al., 2021). We determined that the footprint of the X-ray emission has roughly 1 km radius, and we estimate (in the Appendices) that we should be able to record ∼10–20 strikes per year within this distance of our instrument.

5 Acknowledgments

This research has been supported by NSF grant AGS-1917069 to New Mexico Tech. We thank Earth Networks for providing lightning location data. Data is publicly available at Contreras-Vidal et al. (2023).

References

Abbasi et al., R. U. (2018). Gamma ray showers observed at ground level in coincidence with downward lightning leaders. *J. Geophys. Res.*, *123*. doi: 10.1029/2017JD027931

Abbasi et al., R. U. (2023). First high-speed video camera observations of a lightning flash associated with a downward terrestrial gamma-ray flash. *Geophys. Res. Lett.*, *50*(14), e2023GL102958. doi: 10.1029/2023GL102958

Akita, M., Stock, M., Kawasaki, Z., Krehbiel, P., Rison, W., & Stanley, M. (2014). Data processing procedure using distribution of slopes of phase differences for broadband VHF interferometer. *Journal of Geophysical Research: Atmospheres*, *119*(10), 6085-6104. Retrieved from `https://`

agupubs.onlinelibrary.wiley.com/doi/abs/10.1002/2013JD020378 doi: https://doi.org/10.1002/2013JD020378

Arabshahi, S., Dwyer, J. R., Cramer, E. S., Grove, J. E., Gwon, C., Hill, J. D., ... Rassoul, H. K. (2015). The energy spectrum of x-rays from rocket-triggered lightning. *Journal of Geophysical Research: Atmospheres*, *120*(20), 10,951-10,963. Retrieved from https://agupubs.onlinelibrary.wiley.com/doi/abs/10.1002/2015JD023217 doi: https://doi.org/10.1002/2015JD023217

Belz et al., J. W. (2020). Observations of the origin of downward terrestrial gamma-ray flashes. *J. Geophys. Res. Atmos.*, *125*(23), e2019JD031940. doi: 10.1029/2019JD031940

Biagi, C. J., Uman, M. A., Hill, J. D., Jordan, D. M., Rakov, V. A., & Dwyer, J. (2010). Observations of stepping mechanisms in a rocket-and-wire triggered lightning flash. *Journal of Geophysical Research: Atmospheres*, *115*(D23). Retrieved from https://agupubs.onlinelibrary.wiley.com/doi/abs/10.1029/2010JD014616 doi: https://doi.org/10.1029/2010JD014616

Celestin, S., Xu, W., & Pasko, V. P. (2015). Variability in fluence and spectrum of high-energy photon bursts produced by lightning leaders. *J. Geophys. Res. Space Phys.*, *120*(12), 10,712-10,723. doi: 10.1002/2015JA021410

Christian, H., Holmes, C. R., Bullock, J. W., Gaskell, W., Illingworth, A. J., & Latham, J. (1980). Airborne and ground-based studies of thunderstorms in the vicinity of langmuir laboratory. *Quarterly Journal of the Royal Meteorological Society*, *106*(447), 159-174. Retrieved from https://rmets.onlinelibrary.wiley.com/doi/abs/10.1002/qj.49710644711 doi: https://doi.org/10.1002/qj.49710644711

Contreras-Vidal, L., da Silva, C. L., & Sonnenfeld, R. G. (2022, dec). Production of runaway electrons and x-rays during streamer inception phase. *Journal of Physics D: Applied Physics*, *56*(5), 055201. Retrieved from https://dx.doi.org/10.1088/1361-6463/acaab9 doi: 10.1088/1361-6463/acaab9

Contreras-Vidal, L., Sanchez, J., da Silva, C. L., Sonnenfeld, R., Aulich, G., Edens, H., ... Smith, D. (2023, November). *Preliminary data on the energy distribution of X- and gamma-rays from natural lightning.* Zenodo. Retrieved from https://doi.org/10.5281/zenodo.10085302 doi: 10.5281/zenodo.10085302

Contreras-Vidal, L., Sonnenfeld, R. G., da Silva, C. L., McHarg, M. G., Jensen, D., Harley, J., ... Stenbaek-Nielsen, H. (2021). Relationship between sprite current and morphology. *Journal of Geophysical Research: Space Physics*, *126*(3), e2020JA028930. Retrieved from https://agupubs.onlinelibrary.wiley.com/doi/abs/10.1029/2020JA028930 (e2020JA028930 2020JA028930) doi: https://doi.org/10.1029/2020JA028930

d'Angelo, N. (1987). On x-rays from thunderclouds. In *Annales geophysicae, series b-terrestrial and planetary physics* (Vol. 5).

da Silva, C. L., Millan, R. M., McGaw, D. G., Yu, C. T., Putter, A. S., LaBelle, J., & Dwyer, J. (2017, October). Laboratory measurements of X-ray emissions from centimeter-long streamer corona discharges. *Geophys. Res. Lett.*, *44*(21), 11,174–11,183. doi: 10.1002/2017GL075262

da Silva, C. L., Winn, W. P., Taylor, M. C., Aulich, G. D., Hunyady, S. J., Eack, K. B., ... Trueblood, J. J. (2023). Polarity asymmetries in rocket-triggered lightning. *Geophys. Res. Lett.*, *50*(17), e2023GL105041. doi: 10.1029/2023GL105041

Dwyer, J. R. (2004). Implications of x-ray emission from lightning. *Geophysical Research Letters*, *31*(12). Retrieved from https://agupubs.onlinelibrary.wiley.com/doi/abs/10.1029/2004GL019795 doi: https://doi.org/10.1029/2004GL019795

Dwyer, J. R. (2008). Source mechanisms of terrestrial gamma-ray flashes. *J. Geophys. Res.*, *113*(D10103). doi: 10.1029/2007JD009248

Dwyer, J. R., Rassoul, H. K., Al-Dayeh, M., Caraway, L., Wright, B., Chrest, A., ... Smyth, C. (2004). Measurements of x-ray emission from rocket-triggered lightning. *Geophysical Research Letters*, *31*(5). Retrieved from https://agupubs.onlinelibrary.wiley.com/doi/abs/10.1029/2003GL018770 doi: https://doi.org/10.1029/2003GL018770

Dwyer, J. R., & Smith, D. M. (2005). A comparison between Monte Carlo simulations of runaway breakdown and terrestrial gamma-ray flash observations. *Geophys. Res. Lett.*, *32*(22), L22804. doi: 10.1029/2005GL023848

Dwyer, J. R., Uman, M. A., Rassoul, H. K., Al-Dayeh, M., Caraway, L., Jerauld, J., ... Wright, B. (2003). Energetic radiation produced during rocket-triggered lightning. *Science*, *299*(5607), 694-697. Retrieved from https://www.science.org/doi/abs/10.1126/science.1078940 doi: 10.1126/science.1078940

Eack, K. B., Aulich, G., Rison, W., Edens, H., Hunyady, S., & Winn, W. (2006, December). Gamma-ray emissions from natural dart-leaders. *Presented at the 2006 American Geophysical Union (AGU) Fall Meeting*. (Abstract AE31A-1031)

Gurevich, A. V., Milikh, G. M., & Roussel-Dupré, R. (1992, June). Runaway electron mechanism of air breakdown and preconditioning during a thunderstorm. *Phys. Lett. A*, *165*(5-6), 463-468. doi: 10.1016/0375-9601(92)90348-P

Hill, J. D., Uman, M. A., Jordan, D. M., Dwyer, J. R., & Rassoul, H. (2012). "Chaotic" dart leaders in triggered lightning: Electric fields, X-rays, and source locations. *J. Geophys. Res. Atmos.*, *117*(D3), D03118. doi: 10.1029/2011JD016737

Howard, J., Uman, M. A., Dwyer, J. R., Hill, D., Biagi, C., Saleh, Z., ... Rassoul, H. K. (2008). Co-location of lightning leader x-ray and electric field change sources. *Geophysical Research Letters*, *35*(13). Retrieved from https://agupubs.onlinelibrary.wiley.com/doi/abs/10.1029/2008GL034134 doi: https://doi.org/10.1029/2008GL034134

Jensen, D. P., Sonnenfeld, R. G., Stanley, M. A., Edens, H. E., da Silva, C. L., & Krehbiel, P. R. (2021). Dart-leader and k-leader velocity from initiation site to termination time-resolved with 3d interferometry. *Journal of Geophysical Research: Atmospheres*, *126*(9), e2020JD034309. Retrieved from https://agupubs.onlinelibrary.wiley.com/doi/abs/10.1029/2020JD034309 (e2020JD034309 2020JD034309) doi: https://doi.org/10.1029/2020JD034309

Kereszy, I. (2021). A study of energetic radiation from lightning using ground- and aircraft-based detectors and associated modeling. *Univerity of Florida*, *Dissertation*.

Lapierre, J. L., Sonnenfeld, R. G., Edens, H. E., & Stock, M. (2014). On the relationship between continuing current and positive leader growth. *Journal of Geophysical Research: Atmospheres*, *119*(22), 12–479.

Mallick, S., Rakov, V. A., & Dwyer, J. R. (2012). A study of x-ray emissions from thunderstorms with emphasis on subsequent strokes in natural lightning. *Journal of Geophysical Research: Atmospheres*, *117*(D16). Retrieved from https://agupubs.onlinelibrary.wiley.com/doi/abs/10.1029/2012JD017555 doi: https://doi.org/10.1029/2012JD017555

Moore, C. B., Eack, K. B., Aulich, G. D., & Rison, W. (2001). Energetic radiation associated with lightning stepped-leaders. *Geophysical Research Letters*, *28*(11), 2141-2144. Retrieved from https://agupubs.onlinelibrary.wiley.com/doi/abs/10.1029/2001GL013140 doi: https://doi.org/10.1029/2001GL013140

Moore, C. B., & Vonnegut, B. (1977). The Thundercloud. In R. H. Golde (Ed.), *Lightning: Physics of lightning, volume 1 & 2* (p. 51-98). Academic Press.

Moss, G. D., Pasko, V. P., Liu, N., & Veronis, G. (2006). Monte carlo model for analysis of thermal runaway electrons in streamer tips in transient lu-

minous events and streamer zones of lightning leaders. *Journal of Geophysical Research: Space Physics*, *111*(A2). Retrieved from https://agupubs.onlinelibrary.wiley.com/doi/abs/10.1029/2005JA011350 doi: https://doi.org/10.1029/2005JA011350

Pantuso, J. G., da Silva, C. L., Sanchez, J. T., & Bowers, G. S. (2022). Geant4 simulations of x-ray photon pileup produced by runaway electrons in streamer discharges. *Physics of Plasmas*, *29*(5), 053506. doi: 10.1063/5.0086579

Rison, W., Krehbiel, P. R., Stock, M. G., Edens, H. E., Shao, X.-M., Thomas, R. J., ... Zhang, Y. (2016). Observations of narrow bipolar events reveal how lightning is initiated in thunderstorms. *Nat. Commun.*, *7*(10721). doi: 10.1038/ncomms10721

Saleh, Z., Dwyer, J., Howard, J., Uman, M., Bakhtiari, M., Concha, D., ... Rassoul, H. (2009). Properties of the x-ray emission from rocket-triggered lightning as measured by the thunderstorm energetic radiation array (tera). *Journal of Geophysical Research: Atmospheres*, *114*(D17). Retrieved from https://agupubs.onlinelibrary.wiley.com/doi/abs/10.1029/2008JD011618 doi: https://doi.org/10.1029/2008JD011618

Schaal, M. M., Dwyer, J. R., Saleh, Z. H., Rassoul, H. K., Hill, J. D., Jordan, D. M., & Uman, M. A. (2012). Spatial and energy distributions of x-ray emissions from leaders in natural and rocket triggered lightning. *Journal of Geophysical Research: Atmospheres*, *117*(D15). Retrieved from https://agupubs.onlinelibrary.wiley.com/doi/abs/10.1029/2012JD017897 doi: https://doi.org/10.1029/2012JD017897

Smith, D. M., Bowers, G. S., Kamogawa, M., Wang, D., Ushio, T., Ortberg, J., ... Stock, M. (2018). Characterizing upward lightning with and without a terrestrial gamma ray flash. *J. Geophys. Res. Atmos.*, *123*(20), 11,321-11,332. doi: 10.1029/2018JD029105

Smith, D. M., Ortberg, J., & Chaffin, J. M. (2019, December). New instrumentation for ground and airborne high-energy observations. , *2019*, AE41B-3157.

Tran, M. D., Kereszy, I., Rakov, V. A., & Dwyer, J. R. (2019). On the role of reduced air density along the lightning leader path to ground in increasing X-ray production relative to normal atmospheric conditions. *Geophys. Res. Lett.*, *46*(15), 9252-9260. doi: 10.1029/2019GL083753

Urbani, M., Montanyà, J., van der Velde, O. A., López, J. A., Arcanjo, M., Fontanes, P., ... Roncancio, J. A. (2021). High-energy radiation from natural lightning observed in coincidence with a vhf broadband interferometer. *Journal of Geophysical Research: Atmospheres*, *126*(7), e2020JD033745. Retrieved from https://agupubs.onlinelibrary.wiley.com/doi/abs/10.1029/2020JD033745 (e2020JD033745 2020JD033745) doi: https://doi.org/10.1029/2020JD033745

Xu, W., Marshall, R. A., Celestin, S., & Pasko, V. P. (2017). Modeling of X-ray images and energy spectra produced by stepping lightning leaders. *J. Geophys. Res. Atmos.*, *122*(21), 11,776-11,786. doi: 10.1002/2016JD026410

Zhu, Y., Rakov, V. A., Tran, M. D., Stock, M. G., Heckman, S., Liu, C., ... Hare, B. M. (2017). Evaluation of ENTLN performance characteristics based on the ground truth natural and rocket-triggered lightning data acquired in florida. *Journal of Geophysical Research: Atmospheres*, *122*(18), 9858-9866. Retrieved from https://agupubs.onlinelibrary.wiley.com/doi/abs/10.1002/2017JD027270 doi: https://doi.org/10.1002/2017JD027270

Appendix A Data log

Table A1 contains a list of flashes that triggered our data acquisition system (DAS). The top section shows all flashes that triggered the DAS during the August 9, 2022 thunderstorm, while the bottom section contains two additional flashes with X-ray emissions recorded during different days that Summer. The system triggered on 9 flashes during the August 9 storm, but only two produced detectable X-rays (all are marked with vertical lines in Figure 4). In Table A1, for flashes that did not produce X-rays, we only display basic information pertinent to the entire flash, such as mean distance to sensors, largest peak current, and peak field change. Meanwhile, for flashes that produced X-rays, we show this information for the actual strikes that produced X-rays, as well as information on the properties of the X-rays detected with the LaBr scintillator. There are 11 strikes with associated X-ray data. Four of them were preceded by stepped leaders (A1, B2, C1, and D1), while the other 7 were preceded by dart leaders. The peak field change reported on Table A1 was measured with the calibrated slow antenna.

On the seventh column in Table A1 we report the number of X-ray photons detected in association with each stroke. We estimate that all of these photons are due to the descending lightning leaders, and none of them are from background emissions. Recall that the background emission rate observed with the LaBr detector is 1 photon every 3 ms. The probability that k photons (out of the total) correspond to background emissions in a given time interval Δt can be calculated using the Poisson distribution: $P(k, \Delta t) = (\lambda \Delta t)^k e^{-\lambda \Delta t}/k!$ (e.g., Urbani et al., 2021). Thus, as an example, for event A2, the probability that one or more photons correspond to background is $P(k \geq 1,\, 30\,\mu s) \leq 1\%$. Meanwhile for all events in the table, this probability is given by $P(k \geq 1,\, 1.5\,\text{ms}) \leq 30\%$. If we repeat these calculations for the probability that 2 or more photons arise from background emissions, these percentages are further reduced to 0.005% and 8%, respectively.

Figure A1 shows the distribution of lightning strikes around South Baldy peak during the Summer of 2022. The distribution is plotted as a function of distance (d) to the detectors and peak current (I_p). The figure also marks the bins that contain the strikes from Table A1 that produced X-rays. Based on this figure, and also on a similar analysis done by Kereszy (2021, Figure 3-11), we conclude that high probability of X-ray detection exists for strikes with $d < 1$ km and $I_p > 20$ kA. We have managed to collect data on 8 of the 20 strikes within this range (plus 3 other strikes with lower peak current). To guide future campaigns at the same site, we will use the 10-20 strikes per year figure to estimate how much X-ray data may be collected in a season. Referring back to the August 9 storm, we can see that the other DAS triggers that did not contain X-rays correspond to flashes that took place more than 1.2 km away from South Baldy peak.

Appendix B Flash B

A second flash was detected during the August 9, 2022 storm, which had X-ray emissions. Three stepped leaders (events B1, B2, and B3) and subsequent dart leaders (events B4 to B9) can be distinguished in Figure B1a. An analysis of the location of the strikes allowed us to group events B1 and B3 to B9 to nearby striking points, i.e., subsequent strokes B4 to B9 reuse the channels created by either the B1 or B3 stepped leaders, which touch the ground very close to each other, within the uncertainty of ENTLN. Meanwhile, event B2 corresponds to a stepped leader that made ground contact at a separate location (>1 km away from the rest). The maximum photon energy was 744 keV and corresponded to event B4, a dart leader. Photon count was similar between the stepped and two of the dart leaders, as reported in Table A1.

A zoom into event B2 (Figure B2) shows a complex temporal structure. Thirteen out of the 14 photons detected (in the LaBr scintillator) prior to the return stroke were counted as being emitted by the descending leaders, since they were highly correlated

			ENTLN		Slow antenna	X-rays photons recorded in the LaBr detector		
Event	**Date**	**Time (UTC)**	**Distance (km)**	**Peak current (kA)**	**Peak E-field (kV/m)**	**Number of photons detected**	**Avg. energy (keV)**	**Max. energy (keV)**
August 9 storm								
	08-09-22	17:38:56	2.8	-14	15.6	-	-	-
	08-09-22	17:40:20	1.2	-17	9.4	-	-	-
	08-09-22	17:41:51	1.5	-32	13.2	-	-	-
A1 (stepped)	08-09-22	17:44:02	0.5	-95	15.9	87	416	3801
A2 (dart)	08-09-22	17:44:02	0.5	-50	2.8	64	138	969
	08-09-22	17:54:18	4.6	7	-4.7	-	-	-
	08-09-22	17:55:09	3.8	-10	5.3	-	-	-
B2 (stepped)	08-09-22	17:56:03	0.4	-25	12.3	13	88	212
B4 (dart)	08-09-22	17:56:03	0.5	-20	2.9	12	125	744
B5 (dart)	08-09-22	17:56:03	0.5	-20	2.2	12	101	359
B8 (dart)	08-09-22	17:56:03	0.5	-10	2.2	4	31	44
	08-09-22	17:57:12	2.5	-14	2.5	-	-	-
	08-09-22	18:03:15	1.9	-25	6.7	-	-	-
Other triggers								
C1 (stepped)	07-11-22	17:53:52	0.5	-34	20	6	629	2224
C2 (dart)	07-11-22	17:53:52	0.2	-10	7	6	67	211
C4 (dart)	07-11-22	17:53:52	0.6	-6	3.5	5	38	47
D1 (stepped)	07-31-22	23:38:25	0.4	-27	12	9	125	411
D2 (dart)	07-31-22	23:38:25	0.2	-21	12.5	16	249	1158

Table A1. Summary of flashes recorded with our X-ray detection system. Events labelled on the first column are the ones with associated X-ray emissions, and are scrutinized per stroke/leader type. All other events from the August 9, 2022 storm did not produce detectable X-rays. The last 3 columns display the X-ray data, including, from left-to-right, the number of X-ray photons detected, the average, and the maximum photon energies.

manuscript submitted to *JGR: Atmospheres*

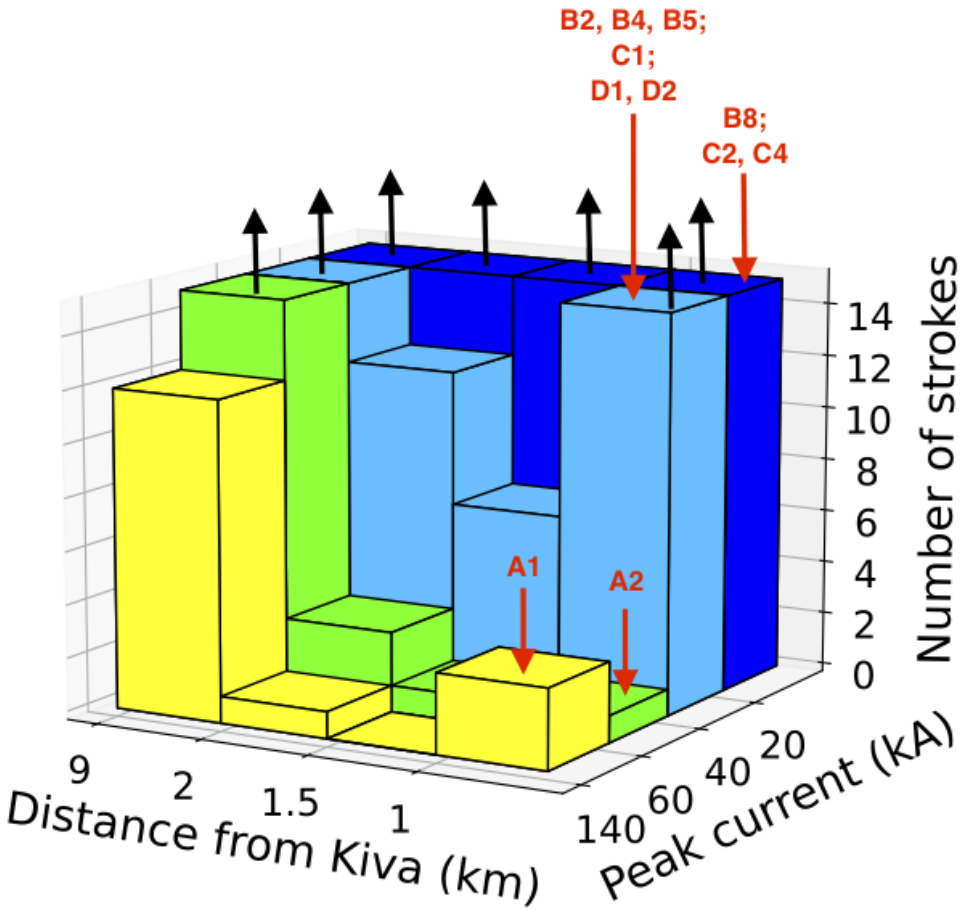

Figure A1. Distribution of lightning strikes that took place within a 9-km radius of South Baldy peak during the Summer of 2022, based on ENTLN data. The black upward arrows mark cropped bins with more than 14 strikes. The red downward arrows mark the locations in the histogram of the events in Table A1 with X-ray detections. The format is similar to Kereszy (2021, Figure 3-11).

to fast antenna field changes. We estimate that 1 photon (or perhaps 2 at the most) during that period is (are) associated with background emissions. Figure B2 and the remaining figures in the Appendices have the same format as Figures 5–7 in the main text. They show the electric field in the top panel (a) with the slow antenna in red, and fast antenna in black (if data is available). LEFA was down during the three flashes reported in the Appendices. The top panels also show the X-ray energies and time of arrival of individual photons, with the LaBr detector shown in blue, while the NaI detector data in orange. The bottom panels (b) display a histogram of the X-ray count rate, using the same color scheme as above to distinguish the two detectors.

Appendix C Flashes C and D

Figures C1 and C2 show flashes C and D, which occurred on July 11 and 31, respectively. Thus, they are not related to the storm discussed in detail in this manuscript. In terms of detectability, flash C is a marginal case with just 5–6 photons per strike. Nonetheless, we can see a similar pattern between its stepped leader (C1) and the one from the

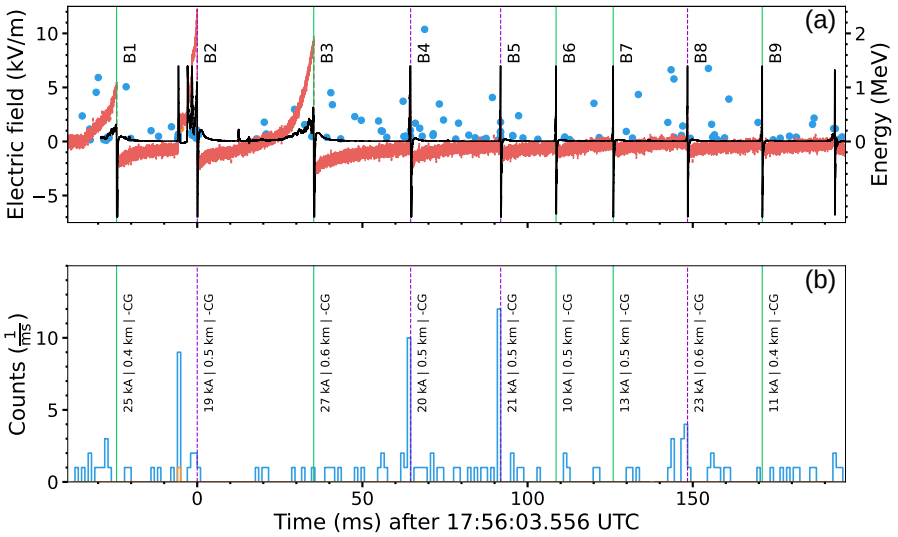

Figure B1. Electric field and X-ray data for flash B. (a) Data from (fast and slow) electric field antennas, as well as both X-ray detectors. (b) Photon count rate histogrammed in 1-ms bins. The figure uses the same color scheme for different instruments as Figures 5–7 in the main text.

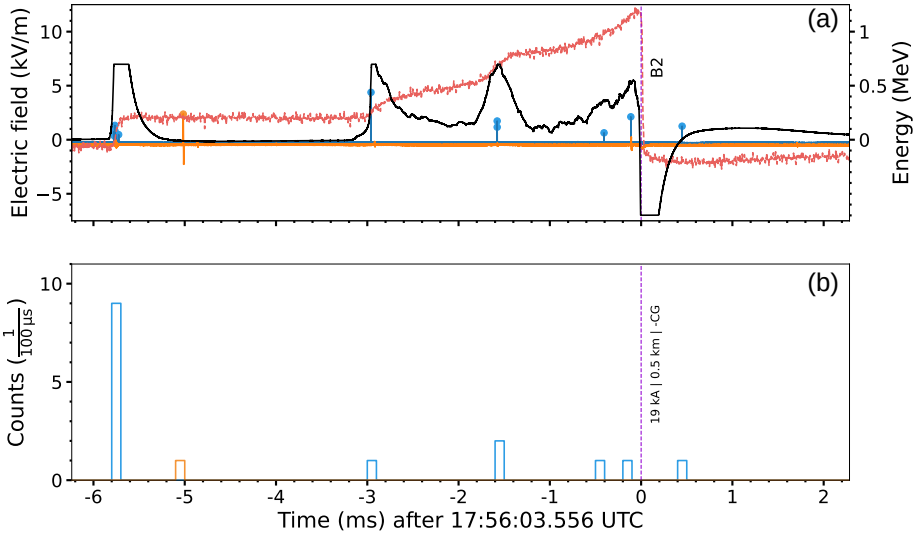

Figure B2. A zoom into event into event B2. An X-ray burst is observed early in the stepped leader phase at $t = -5.8$ ms. The average photon energy of this burst is 88 keV, while the maximum is 212 keV. The figure has the same format and color scheme as Figures 5–7 in the main text.

729 previous flash (B2). Both display a clear X-ray burst (above background levels) at the
730 very beginning of the stepped leader field change, a few ms before the return stroke.

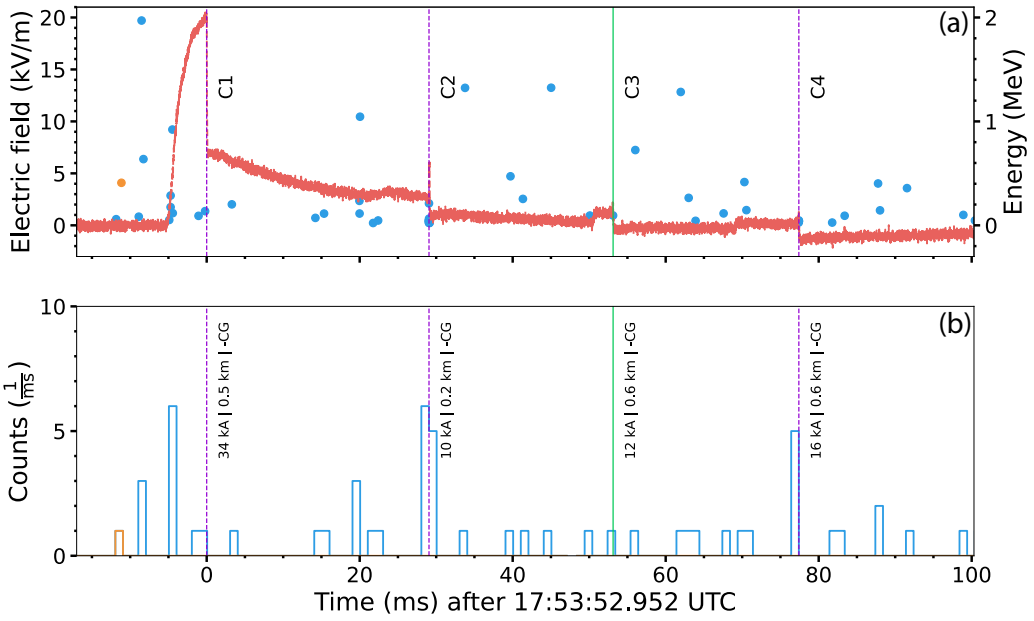

Figure C1. Electric field and X-ray data for flash C, which took place on July 11, 2022. The figure has the same format and color scheme as Figures 5–7 in the main text. Figures C1 and C2 do not display the fast antenna and LEFA records because the antennas were down during these particular triggers.

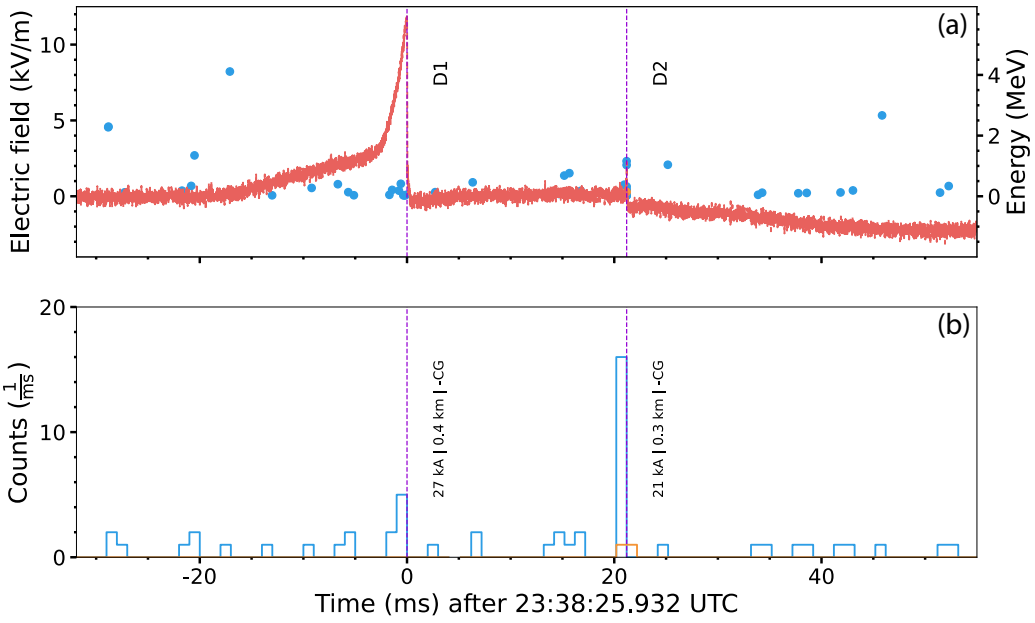

Figure C2. Electric field and X-ray data for flash D, which took place on July 31, 2022. The figure has the same format and color scheme as Figures 5–7.

731 The maximum photon energy detected for flashes C and D was 2.2 and 1.2 MeV,
732 respectively. In both cases the photons with highest energies were produced by their re-

spective stepped leaders. Flash D (in Figure C2) is the only clear case in our data set where a subsequent-stroke leader was a more-prolific X-ray emitter than the first-stroke leader. In all flash overview figures (Figs. 5, B1, C1, and C2), the background count rate of 1 photon every 3 ms can be easily observed in between strikes. For all return strokes with associated X-ray observations, all photons were detected during the preceding leader phase (within the level of uncertainty of relative timing across our data sets). In all figures where non-colocated instruments are lined up, a correction for the speed of light (c) travel between source and instrument is added to the data. We use the frame of reference of the X-ray instrument in all plots. Thus, before overlaying the ENTLN strike data to the plots, we delay its arrival by an amount d/c. For flashes located around $d = 1$ km from South Baldy peak, this delay has a 10–20% uncertainty (<1 μs, arising from location uncertainty).